Thin-Walled Structures 123 (2018) 509–519

Contents lists available at ScienceDirect

Thin-Walled Structures

journal homepage: www.elsevier.com/locate/tws

Full length article

Analytical solution for cylindrical bending of two-layered corrugated and webcore sandwich panels

Anup Pydah, R.C. Batra*

Department of Biomedical Engineering and Mechanics, Virginia Polytechnic Institute and State University M/C 0219, Blacksburg, VA 24061, USA

ARTICLE INFO

Keywords:
Sandwich panels
Webcore
Corrugated core
Analytical solution
Curvature changes
Oscillatory axial stress

ABSTRACT

We analytically investigate infinitesimal cylindrical bending deformations of two-layered triangular corrugated and webcore linearly elastic sandwich panels by using the mechanics of materials approach and the classical plate theory. The model is validated by comparing its predictions with the solution by the finite element method of the linear elasticity equations for plane strain deformations. The model can accurately capture the secondary bending of the facesheets, manifested as changes in their curvature between the webs and the resulting changes in the axial stresses, from being tensile to possibly compressive, that the commonly-employed homogenization schemes fail to capture. Subsequently, the model is used to analyze several problems with the sandwich panel having a pinned support at the left edge and a roller support at the right edge, and a uniformly distributed load applied on the top facesheet of the panel. It is found that the core plates mostly deform in compression and bending, respectively, for corrugated and web core panels. Furthermore, a significant fraction of the work done by the external load on the structure is absorbed as strain energy of deformations of the core plates near the supports. For four hybrid combinations of corrugated and webcore configurations in two-layered panels, the combination with the upper corrugated core set-up has the least maximum face sheet deflection and axial stress. The analytical technique can be easily extended to multi-layered hybrid configurations and provides quick means of finding efficient strain-energy absorbing hybrid designs.

1. Introduction

Sandwich panels possess high stiffness-to-weight ratios making them a popular choice in aerospace, naval and automobile industries. Discrete core sandwich plates [1] with corrugated cores or webcores (see Fig. 1) or other cellular configurations offer good crash-worthiness and blast-mitigation properties and can be tailored to meet various design requirements.

The mechanical response of a sandwich plate is commonly analyzed by using continuum-based homogenized models wherein an equivalent homogeneous orthotropic layer replaces a discrete Z-core [2,3], webcore [4–6], chevron foldcore [7] or corrugated core [8–13]. The equivalent mechanical properties of the homogeneous layer are determined by using either an energy-based approach [14,15], or a micromechanics theory [16] or an asymptotic expansion method [17]. The accuracy of these schemes is established by comparing predictions from the homogenized models with those from the numerical solution of the linear elasticity equations governing deformations of facesheets and the core usually by the finite element method (FEM). These studies [18,19] have revealed the sensitivity of the sandwich panel response to small variations in the effective material properties of the homogeneous layer. They have shown that predicting the local response like secondary bending of the panel between the webs for accurate stress and displacement results requires a discrete modeling approach [20]. Furthermore, expressions for the effective material properties developed for one core configuration cannot be generally used for other core designs [21]. Detailed numerical simulations characterizing the response of corrugated sandwich panels [22–25] require considerable computational effort and expense that increases with the size and the complexity of the core configuration.

For *single-core* sandwich panels, analytical models have been developed that analyze the discrete structural core [4,26,27], and are based on a superposition of global panel deformations on the local frame response. They neglect the lateral bending and twisting of webs. Analytical models have been developed [20,28] for simply supported webcore sandwich plates wherein facesheets are analyzed by using equations of the three-dimensional linear elasticity and the webs as a combination of two-dimensional plane stress analysis and the Euler-Bernoulli beam theory.

Two-layered (dual-core) or multi-core sandwich panels consisting of

* Corresponding author.
E-mail addresses: anpydah@vt.edu (A. Pydah), rbatra@vt.edu (R.C. Batra).

https://doi.org/10.1016/j.tws.2017.11.023
Received 7 August 2017; Received in revised form 12 October 2017; Accepted 13 November 2017

two or more core layers separated by metallic or composite facesheets have been shown to be superior to equal areal density single-core structures in terms of their impact resistance [29], energy absorption [30] and sound-absorbing capabilities [31]. However, with many studies using FE simulations, there is a need for analytical solutions for multi-layered corrugated sandwich panels which can accurately capture local effects like secondary bending of the face-plates between the webs and can be used for design/optimization studies.

The objective of the current work is to analytically study linearly elastic plane strain deformations of two-layered corrugated sandwich panels. Facesheets and core web plates are modeled using kinematic assumptions of the Love-Kirchhoff plate theory, usually called the classical plate theory (CPT) and enforcing the continuity of displacements and tractions at interfaces between web plates and facesheets which are assumed to be perfectly bonded. The model can accurately capture secondary bending effects in facesheets such as changes in the axial stress field from being compressive to possibly tensile for a uniformly distributed normal surface traction on the top facesheet as well as sudden changes in the curvature of the facesheet between the web plates. For single-layered corrugated panels, it is shown that the corrugated core web plates deform in compression while for webcore sandwich panels, they deform in bending. Furthermore, for simply supported panels, a significant fraction of the work done by the external load on the structure is absorbed by the elastic deformations of the web plates near the pin and roller supports.

Four hybrid configurations of two-layered sandwich panels designed as combinations of corrugated and webcores of equal areal density under the action of a uniformly distributed normal surface traction are compared in terms of the total strain energy of the core webs, facesheet deflections and axial stresses. Results indicate that webcore configurations absorb a greater fraction of the work done by external forces while corrugated-based designs have lesser facesheet deflections and axial stresses. The modeling approach can be extended to multi-layered sandwich panels for quick and accurate design and optimization studies.

2. Mathematical model

Fig. 2 shows a two-layered corrugated sandwich panel consisting of three facesheets of length L and thickness h_f separated by two triangular corrugated cores, each of height H. The panel is very wide in the $y-$ direction (width $\gg L$) and is subjected to a transverse load that does not vary along its width. The left ends ($x = 0$) of the facesheets are pinned while the right ends ($x = L$) are supported on rollers. The $xz-$ plane coincides with the mid-surface of the top facesheet in the undeformed reference configuration. The panel is assumed to be in a state of plane strain (in the $xz-$ plane) undergoing cylindrical bending deformations. As shown in Fig. 3, each corrugated core consists of a set of ${}^{D}n$ inclined web plates of thickness ${}^{D}t_i$ and inclination angle ${}^{D}\phi_i$ ($i = 1, 2, ..., {}^{D}n$), measured counter-clockwise from the positive $x-$ axis, which are assumed to be perfectly bonded to the mid-plane of the facesheets at locations ${}^{F}x_i^{D}$ ($i = 1, 2, ..., {}^{D}n$). The superscript D equals $U\,(L)$ to denote the upper (lower) corrugated core, while the superscript F equals T, M and B for the top, the middle and the bottom facesheet, respectively. The notation used to identify the number of corrugated web plates is $\{{}^{U}n \times {}^{L} n\}$. In the present discrete formulation, facesheets and web plates are modeled separately and continuity of forces, moments and displacements is enforced at interfaces where they are attached to each other. Transverse shear deformations are neglected in facesheets and the core web plates as is done in the CPT.

2.1. Mechanics of web plates

As shown in Fig. 4, two interface forces, ${}^{D}P_i^d$ (along the $x-$ direction) and ${}^{D}Q_i^d$ (along the $z-$ direction), and an interface moment ${}^{D}M_i^d$ (about the $y-$ axis) are considered at the top and the bottom edges of the i^{th} web plate. The right superscript d takes values t and b to denote, respectively, the top and the bottom of the web plate. In order to facilitate analysis of each web plate, a local coordinate system $(\overline{x},\ \overline{z})$ is used that is related to the global coordinate axes (x, z) as

$$\begin{Bmatrix} \overline{x} \\ \overline{z} \end{Bmatrix} = \begin{bmatrix} \cos {}^{D}\phi_i & -\sin {}^{D}\phi_i \\ \sin {}^{D}\phi_i & \cos {}^{D}\phi_i \end{bmatrix} \begin{Bmatrix} x \\ z \end{Bmatrix} \tag{1}$$

The transformed interface forces ${}^{D}\overline{P}_i^d$ (along the $\overline{x}-$ direction) and ${}^{D}\overline{Q}_i^d$ (along the $\overline{z}-$ direction), and moment ${}^{D}\overline{M}_i^d$ (about the $y-$ axis) are given by

$$\begin{Bmatrix} {}^{D}\overline{P}_i^d \\ {}^{D}\overline{Q}_i^d \end{Bmatrix} = \begin{bmatrix} \cos {}^{D}\phi_i & -\sin {}^{D}\phi_i \\ \sin {}^{D}\phi_i & \cos {}^{D}\phi_i \end{bmatrix} \begin{Bmatrix} {}^{D}P_i^d \\ {}^{D}Q_i^d \end{Bmatrix}$$
$${}^{D}\overline{M}_i^d = {}^{D}M_i^d \tag{2}$$

Equilibrium equations for the web plate along the $\overline{x}-$ and the $\overline{z}-$ directions and of the moment about the $y-$ axis give relations (3) between the interface forces and moments acting on the top and the bottom of each web plate:

$${}^{D}\overline{P}_i^b = -{}^{D}\overline{P}_i^t,\ \ {}^{D}\overline{Q}_i^b = -{}^{D}\overline{Q}_i^t,\ \ {}^{D}\overline{M}_i^b = -{}^{D}\overline{M}_i^t + {}^{D}\overline{Q}_i^t \frac{H}{\sin {}^{D}\phi_i} \tag{3}$$

Kinematic assumptions of the CPT, i.e., cross-section normals to the mid-plane, $\overline{z} = 0$, of the undeformed web plate suffer no change in length and remain normal to the deformed mid-plane, imply the following displacement field

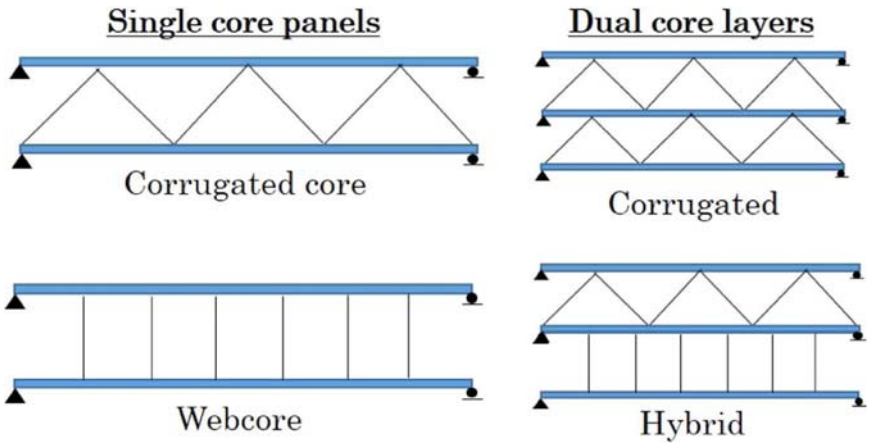

Fig. 1. Sandwich core configurations.

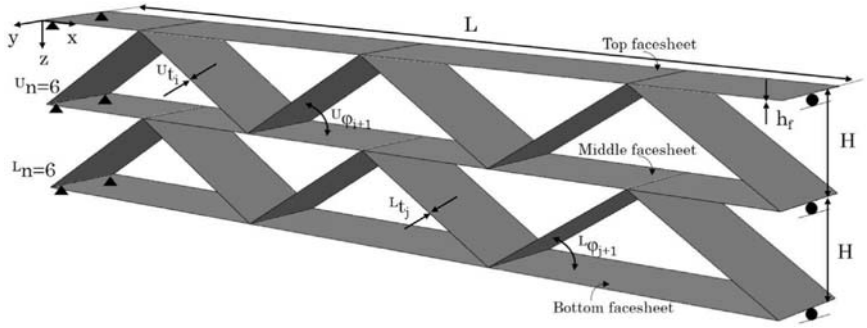

Fig. 2. Two-layered (dual-core) corrugated sandwich plate.

$$
\begin{aligned}
&{}^{D}\overline{w}_i(\overline{x}, y, \overline{z}) = {}^{D}\overline{w}_i^0(\overline{x}) \\
&{}^{D}\overline{u}_i(\overline{x}, y, \overline{z}) = {}^{D}\overline{u}_i^0(\overline{x}) - \overline{z}\frac{d^{D}\overline{w_i^0}}{d\overline{x}}
\end{aligned} \tag{4}
$$

where ${}^{D}\overline{u}_i^0$ and ${}^{D}\overline{w}_i^0$ are the mid-plane displacements of the web plate along the $\overline{x}-$ and the $\overline{z}-$ directions, respectively. Using the expression for the infinitesimal axial strain, $\epsilon_{\overline{x}} = \frac{d^{D}\overline{u_i}}{d\overline{x}}$, and Hooke's law for plane strain deformations, $\epsilon_{\overline{x}} = \frac{1-\nu^2}{E}\sigma_{\overline{x}}$, the axial force ${}^{D}N_i(\overline{x})$ and the bending moment ${}^{D}M_i(\overline{x})$ about the $y-$ axis through the mid point of the web plate thickness are given by

$$
{}^{D}N_i(\overline{x}) = \int_{-\frac{{}^{D}t_i}{2}}^{\frac{{}^{D}t_i}{2}} \sigma_{\overline{x}}(\overline{x}, \overline{z})d\overline{z} = \frac{E\ {}^{D}t_i}{1-\nu^2}\frac{d^{D}\overline{u}_i^0}{d\overline{x}} \tag{5}
$$

$$
{}^{D}M_i(\overline{x}) = \int_{-\frac{{}^{D}t_i}{2}}^{\frac{{}^{D}t_i}{2}} \overline{z}\sigma_{\overline{x}}(\overline{x}, \overline{z})d\overline{z} = -\frac{E\ {}^{D}t_i{}^3}{12(1-\nu^2)}\frac{d^{2D}\overline{w_i^0}}{d\overline{x}^2} \tag{6}
$$

Here E is Young's modulus and ν Poisson's ratio of the web plate material.

The axial force ${}^{D}N_i(\overline{x})$ and the bending moment ${}^{D}M_i(\overline{x})$ at section $\overline{x}$ are given by

$$
{}^{D}N_i = -{}^{D}\overline{P}_i^b,\ {}^{D}M_i = -{}^{D}\overline{M}_i^b - {}^{D}\overline{Q}_i^b\,\overline{x}
$$

Using Eqs. (5) and (6), governing equations for the web plate are

$$
\begin{aligned}
&\frac{E\ {}^{D}t_i}{1-\nu^2}\frac{d^{D}\overline{u}_i^0}{d\overline{x}} = -{}^{D}\overline{P}_i^b \\
&\frac{E\ {}^{D}t_i^3}{12(1-\nu^2)}\frac{d^{2D}\overline{w}_i^0}{d\overline{x}^2} = {}^{D}\overline{M}_i^b + {}^{D}\overline{Q}_i^b\,\overline{x}
\end{aligned} \tag{7}
$$

Integrating the two governing differential Eqs. (7) and using Eqs. (3), the mid-plane displacements of the i^{th} web plate can be determined as

$$
\begin{aligned}
{}^{D}\overline{u}_i^0(\overline{x}) &= \frac{1-\nu^2}{E\ {}^{D}t_i}{}^{D}\overline{P}_i^t\,\overline{x} + {}^{D}W_i^1 \\
{}^{D}\overline{w}_i^0(\overline{x}) &= -\frac{12(1-\nu^2)}{E\ {}^{D}t_i{}^3}\left({}^{D}\overline{M}_i^t\frac{\overline{x}^2}{2} + {}^{D}\overline{Q}_i^t\left(\frac{\overline{x}^3}{6} - \frac{H\overline{x}^2}{2\sin{}^{D}\phi_i}\right)\right) \\
&\quad + {}^{D}W_i^2\overline{x} + {}^{D}W_i^3
\end{aligned} \tag{8}
$$

where ${}^{D}W_i^j$ $(j = 1, 2, 3)$ are constants. The displacement field $({}^{D}u_i(x, z),\ {}^{D}w_i(x, z))$ of each web in the global coordinate system (x, y, z) can be determined in terms of loads ${}^{D}P_i^d$, ${}^{D}Q_i^d$ and the moment ${}^{D}M_i^d$ by using Eqs. (2) and (4) and the transformation rules for vectors.

2.2. Equilibrium equations for facesheets

As shown in Fig. 4, each facesheet is also subjected to interface

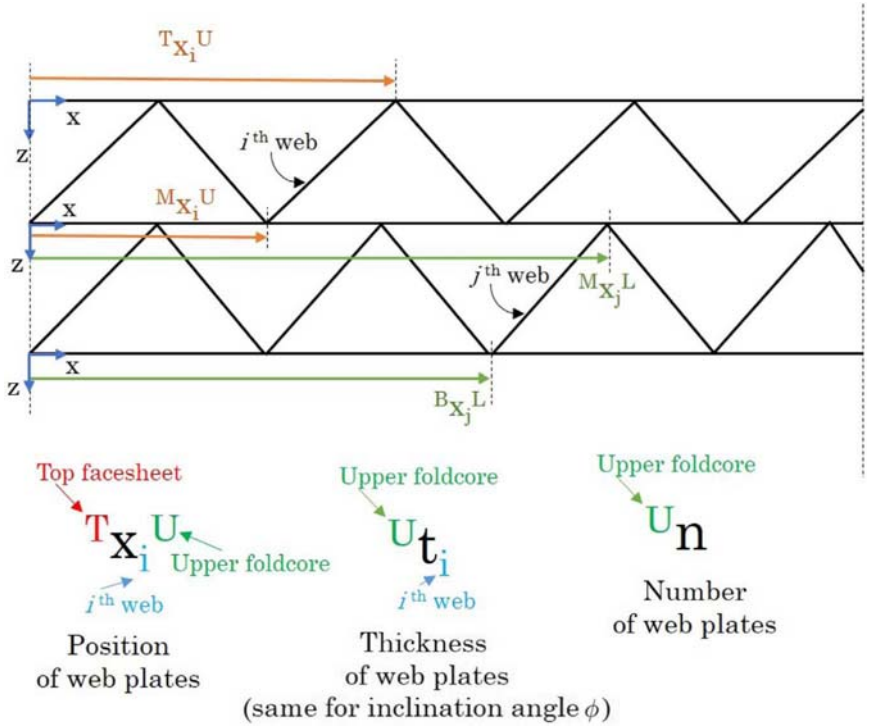

Fig. 3. Explanation of notations in a section of the sandwich panel.

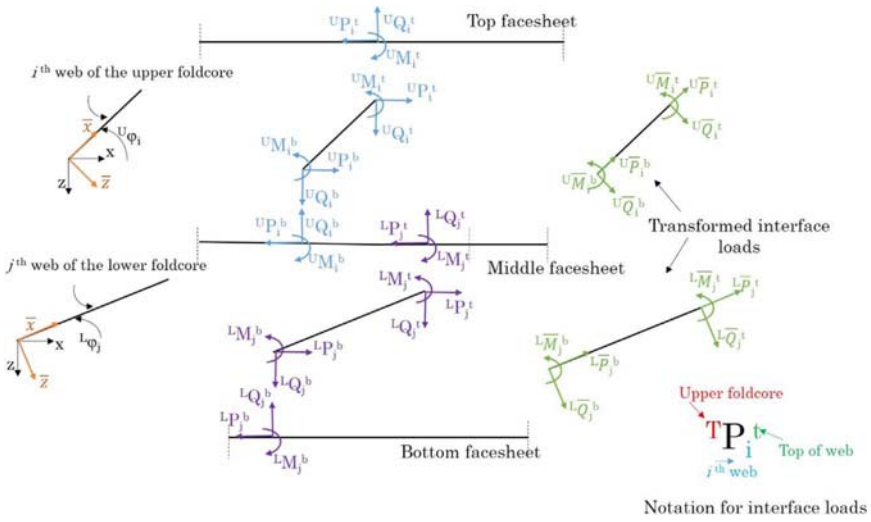

Fig. 4. Forces and moments on different members.

forces and moments from the attached web plates. The loads on each facesheet, except that from the supports, are summarized below.

- Top facesheet: Point forces ${}^{U}P_i^t$ and ${}^{U}Q_i^t$ and moments ${}^{U}M_i^t$ acting at locations ${}^{T}x_i$ $(i = 1, 2, ..., {}^{U}n)$ and externally applied normal surface traction ${}^{T}q(x)$ taken positive downwards.
- Middle facesheet: Point forces ${}^{U}P_i^b$ and ${}^{U}Q_i^b$ and moments ${}^{U}M_i^b$ acting at locations ${}^{M}x_i$ $(i = 1, 2, ..., {}^{U}n)$, point forces ${}^{L}P_j^t$ and ${}^{L}Q_j^t$ and moments ${}^{L}M_j^t$ acting at locations ${}^{M}x_j$ $(j = 1, 2, ..., {}^{L}n)$ and externally applied normal surface traction ${}^{M}q(x)$ taken positive downwards.
- Bottom facesheet: Point forces ${}^{L}P_j^b$ and ${}^{L}Q_j^b$ and moments ${}^{L}M_j^b$ acting at locations ${}^{B}x_j$ $(j = 1, 2, ...L_n)$ and externally applied normal surface traction ${}^{B}q(x)$, taken positive downwards.

2.2.1. Top facesheet

The support reactions ${}^{T}R_{x0}$ and ${}^{T}R_{z0}$ at the pinned end, $x = 0$, in the $x-$ and the $z-$ directions are

$$
\begin{aligned}
{}^{T}R_{x0} &= -\sum_{j=1}^{{}^{U}n} {}^{U}P_j^t \\
{}^{T}R_{z0} &= \frac{1}{L}\left(\int_0^{L} {}^{T}q(x)x\,dx - \sum_{j=1}^{{}^{U}n} {}^{U}Q_j^t(L - {}^{T}x_j^U) - \sum_{j=1}^{{}^{U}n} {}^{U}M_j^t\right)
\end{aligned}
$$

The axial force ${}^{T}N_f$ and the bending moment ${}^{T}M_f$ at the section, $x = x^*$, are given by

$$
{}^{T}N_f(x^*) = {}^{T}R_{x0} + \sum_{j=1}^{j^*} \mathrm{H}(x^* - {}^{T}x_j^U)\,{}^{U}P_j^t \tag{9}
$$

$$
\begin{aligned}
{}^{T}M_f(x^*) = {}^{T}R_{z0}\,x^* - \int_0^{x^*} {}^{T}q(x)x\,dx + \sum_{j=1}^{j^*} \mathrm{H}(x^* - {}^{T}x_j^U)\,{}^{U}M_j^t \\
+ \sum_{j=1}^{j^*} \mathrm{H}(x^* - {}^{T}x_j^U)\,{}^{U}Q_j^t(x^* - {}^{T}x_j^U)
\end{aligned} \tag{10}
$$

where j^* is the number of web plates of the upper corrugated core located to the left of the section, $x = x^*$, and $\mathrm{H}(x)$ is the Heaviside function defined as

$$
\mathrm{H}(x - a) = \begin{cases} 0 & x < a \\ 1 & x > a \end{cases}
$$

The derivative of the Heaviside function $\mathrm{H}(x)$ is the unit impulse or the Dirac Delta function $\delta(x)$ defined as

$$
\delta(x - a) = \begin{cases} 0 & x < a \\ \infty & x = a \\ 0 & x > a \end{cases}
$$

2.2.2. Middle facesheet

The support reactions ${}^{M}R_{x0}$ and ${}^{M}R_{z0}$ at the pinned end, $x = 0$, in the $x-$ and the $z-$ directions are

$$
\begin{aligned}
{}^{M}R_{x0} &= -\sum_{j=1}^{{}^{U}n} {}^{U}P_j^b - \sum_{j=1}^{{}^{L}n} {}^{L}P_j^t \\
{}^{M}R_{z0} &= \frac{1}{L}\left(\int_0^{L} {}^{M}q(x)\,x\,dx - \sum_{j=1}^{{}^{U}n} {}^{U}Q_j^b(L - {}^{M}x_j^U) - \sum_{j=1}^{{}^{U}n} {}^{U}M_j^b \right. \\
&\quad \left. - \sum_{j=1}^{{}^{L}n} {}^{L}Q_j^t(L - {}^{M}x_j{}^{L}) - \sum_{j=1}^{{}^{L}n} {}^{L}M_j^t\right)
\end{aligned}
$$

The axial force ${}^{M}N_f$ and the bending moment ${}^{M}M_f$ at the section, $x = x^*$, are given by

$$
{}^{M}N_f(x^*) = {}^{M}R_{x0} + \sum_{j=1}^{j^*} \mathrm{H}(x^* - {}^{M}x_j^U)\,{}^{U}P_j^b + \sum_{k=1}^{k^*} \mathrm{H}(x^* - {}^{M}x_k^L)\,{}^{L}P_k^t \tag{11}
$$

$$
\begin{aligned}
{}^{M}M_f(x^*) &= {}^{M}R_{z0}x^* - \int_0^{x^*} {}^{M}q(x)\,x\,dx + \sum_{j=1}^{j^*} \mathrm{H}(x^* - {}^{M}x_j^U)\,{}^{U}M_j^b \\
&\quad + \sum_{j=1}^{j^*} \mathrm{H}(x^* - {}^{M}x_j^U)\,{}^{U}Q_j^b(x^* - {}^{M}x_j^U) \\
&\quad + \sum_{k=1}^{k^*} \mathrm{H}(x^* - {}^{M}x_k^L)\,{}^{L}M_k^t \\
&\quad + \sum_{k=1}^{k^*} \mathrm{H}(x^* - {}^{M}x_k^L)\,{}^{L}Q_k^t(x^* - {}^{M}x_k^L)
\end{aligned} \tag{12}
$$

where j^* and k^* are the number of web plates of the upper and the lower corrugated core, respectively, located to the left of the section, $x = x^*$.

2.2.3. Bottom facesheet

The support reactions ${}^{B}R_{x0}$ and ${}^{B}R_{z0}$ at the pinned end, $x = 0$, in the $x-$ and the $z-$ directions are

$$ {}^{B}R_{x0} = -\sum_{j=1}^{{}^{L}n} {}^{L}P_j^b $$

$$ {}^{B}R_{z0} = \frac{1}{L}\left(\int_0^L {}^{B}q(x)\, x\, dx - \sum_{j=1}^{{}^{L}n} {}^{L}Q_j^b (L - {}^{B}x_j^L) - \sum_{j=1}^{{}^{L}n} {}^{L}M_j^b \right) $$

The axial force ${}^{B}N_f$ and the bending moment ${}^{B}M_f$ at the section, $x = x^*$, are given by

$$ {}^{B}N_f(x^*) = {}^{B}R_{x0} + \sum_{j=1}^{j^*} \mathrm{H}(x^* - {}^{B}x_j^L) {}^{L}P_j^b \tag{13} $$

$$ \begin{aligned} {}^{B}M_f(x^*) &= {}^{B}R_{z0}x^* - \int_0^{x^*} {}^{B}q(x)\, x\, dx + \sum_{j=1}^{j^*} \mathrm{H}(x^* - {}^{B}x_j^L) {}^{L}M_j^b \\ &\quad + \sum_{j=1}^{j^*} \mathrm{H}(x^* - {}^{B}x_j^L) {}^{L}Q_j^b (x^* - {}^{B}x_j^L) \end{aligned} \tag{14} $$

where j^* is the number of web plates of the bottom corrugated core located to the left of the section, $x = x^*$.

Using the CPT, governing equations for the facesheets are

$$ \frac{Eh_f}{1-\nu^2} \frac{d({}^{F}u_f^0)}{dx^*} = {}^{F}N_f(x^*) \tag{15} $$

$$ -\frac{Eh_f^3}{12(1-\nu^2)} \frac{d^2({}^{F}w_f^0)}{dx^{*2}} = {}^{F}M_f(x^*) \tag{16} $$

where ${}^{F}u_f^0$ and ${}^{F}w_f^0$ are, respectively, the mid-plane displacements of facesheets along the $x-$ and the $z-$ directions.

The solution of the two ordinary differential Eqs. (15) and (16) requires three boundary conditions to be specified: ${}^{F}w_f^0(0) = {}^{F}w_f^0(L) = 0$ and ${}^{F}u_f^0(0) = 0$. We thus get the mid-plane displacements of each facesheet in terms of the unknown interface loads.

2.3. Continuity conditions at interfaces between facesheets and web plates

To ensure continuity of displacements and rotations at interfaces between facesheets and web plates, and to determine the unknown interface forces and moments and constants of integration ${}^{D}W_i^j$ $(j = 1, 2, 3)$, six conditions are specified for each web plate. For example, for the i^{th} web plate in the upper corrugated core:

$$ \begin{aligned} {}^{T}w_f({}^{T}x_i^U, 0) &= {}^{U}w_i(H\cot{}^{U}\phi_i, -H) \\ {}^{T}u_f({}^{T}x_i^U, 0) &= {}^{U}u_i(H\cot{}^{U}\phi_i, -H) \\ \frac{\partial {}^{T}w_f}{\partial x}({}^{T}x_i^U, 0) &= \frac{\partial {}^{U}w_i}{\partial x}(H\cot{}^{U}\phi_i, -H) \\ {}^{M}w_f({}^{M}x_i^U, 0) &= {}^{U}w_i(0, 0) \\ {}^{M}u_f({}^{M}x_i^U, 0) &= {}^{U}u_i(0, 0) \\ \frac{\partial {}^{M}w_f}{\partial x}({}^{M}x_i^U, 0) &= \frac{\partial {}^{U}w_i}{\partial x}(0, 0) \end{aligned} \tag{17} $$

Imposing continuity conditions (17) results in $6({}^{U}n + {}^{L}n)$ linear algebraic equations for the unknown interface forces and moments and constants of integration ${}^{D}W_i^j$ $(j = 1, 2, 3)$ in terms of the applied loads. Displacements, axial forces and bending moments in the web plates are determined using Eqs. (5), (6) and (8).

3. Example problems

Unless otherwise mentioned, we assume that the web plates and the facesheets are made of steel for which $E = 200$ GPa and $\nu = 0.3$. The left ends of the facesheets ($x = 0$) are pinned while the right ends ($x = L$) are supported on rollers. The horizontal reaction force at the left pinned end and the horizontal interface forces at the web plates-facesheet interfaces induce an axial stress in the facesheets. The axial stress exhibited in the figures below is the sum of those due to the axial force and the bending moment at a point. In all example problems studied here, a uniformly distributed normal surface traction is applied on the upper surface of the top facesheet.

3.1. Two-layered {6 × 6} corrugated sandwich panel

Deformations of a two-layered corrugated sandwich panel with $L = 0.1$ m, $h_f = 1$ mm, $H = 1$ cm, ${}^{U}n = {}^{L}n = 6$, ${}^{U}t_i = {}^{L}t_i = h_f/100$ and ${}^{T}q(x) = q_0 = 100$ kN/m are studied. The analytical solution for the mid-plane displacements of the top facesheet in terms of the interface loads is

$$ {}^{T}u_f^0(x) = \frac{1-\nu^2}{Eh_f}\left({}^{T}R_{x0}\, x + \sum_{j=1}^{j^*} \mathrm{H}(x - {}^{T}x_j^U) {}^{U}P_j^t (x - {}^{T}x_j^U) \right) \tag{18} $$

$$ \begin{aligned} {}^{T}w_f^0(x) &= -\frac{12(1-\nu^2)}{Eh_f^3}\left({}^{T}R_{z0}\frac{x^3}{6} + \sum_{j=1}^{j^*} \mathrm{H}(x - {}^{T}x_j^U) {}^{U}M_j^t \frac{(x - {}^{T}x_j^U)^2}{2} \right. \\ &\quad \left. + \sum_{j=1}^{j^*} \mathrm{H}(x - {}^{T}x_j^U) {}^{U}Q_j^t \frac{(x - {}^{T}x_j^U)^3}{6} - q_0\frac{x^4}{24} + C_1 x \right) \end{aligned} \tag{19} $$

where

$$ \begin{aligned} C_1 &= -\frac{1}{L}\left({}^{T}R_{z0}\frac{L^3}{6} + \sum_{j=1}^{6} {}^{U}M_j^t \frac{(x - {}^{T}x_j^U)^2}{2} \right. \\ &\quad \left. + \sum_{j=1}^{6} {}^{U}Q_j^t \frac{(x - {}^{T}x_j^U)^3}{6} - q_0\frac{L^4}{24} \right) \\ {}^{T}R_{y0} &= \frac{1}{L}\left(q_0\frac{L^2}{2} - \sum_{j=1}^{6} {}^{U}Q_j^t (L - {}^{T}x_j^U) - \sum_{j=1}^{6} {}^{U}M_j^t \right) \end{aligned} $$

Here j^* is the number of web plates of the upper corrugated core located to the left of the section at the location x and ${}^{T}x^U = \left\{\frac{L}{6}, \frac{L}{6}, \frac{L}{2}, \frac{L}{2}, \frac{5L}{6}, \frac{5L}{6}\right\}$ are locations of the upper corrugated web plates on the top facesheet.

3.1.1. Comparison with the linear elasticity theory solution

For comparison with the solution of the linear elasticity equations, we analyze plane strain deformations of the sandwich panel by the FEM using the commercial software ABAQUS/ Standard [32]. The facesheets and the web plates are meshed using 8-node shell elements with reduced integration (element S8R). Each facesheet is discretized into 100 uniform elements along the length and 1 element along the width and each web plate is meshed with 20 uniform elements along the $\overline{x}$ direction and 1 element along the width. The core webs are attached to facesheets using the tie constraint which ensures perfect bonding. The sandwich panel is modeled with a finite width $W = \frac{L}{100}$ in the $y-$ direction. Boundary conditions which restrict the y- displacement and rotations about the $x-$ and the $z-$ axes are imposed along edges $y = 0$ and $y = W$ of the panel. For each facesheet, boundary conditions at the pinned edge, $x = 0$, and the roller-supported edge, $x = L$, are modeled as $u(0) = w(0) = w(L) = 0$. The uniformly distributed normal load is applied as a pressure $P_0 = q_0/W = 100$ MPa on the top facesheet. The FE mesh used was found to give converged displacements and stresses within a tolerance of 0.15%. From the FE results, the work done by the applied load was calculated as 0.627 J and was found to equal the strain energy of the structure ensuring that very little, if any, energy was dissipated due to hour glass modes that could ensue because of the reduced integration rule used. The support reactions ${}^{T}R_{x0}$ and ${}^{T}R_{z0}$ at the pinned end, $x = 0$, of the top facesheet were calculated as 695 N and 623 N, respectively, from the FE results and were found to differ from those determined by the analytical solution by less than 1 %.

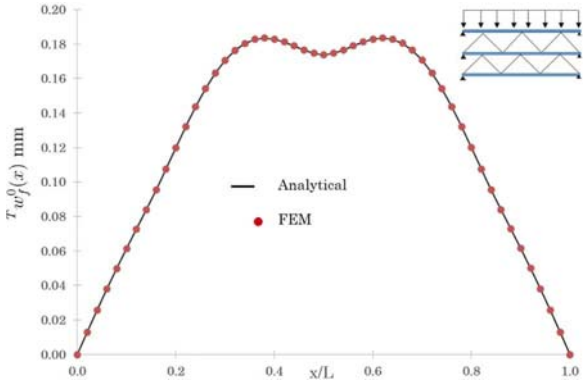

Fig. 5. Variation of the transverse displacement ${}^{T}w_f^0(x)$ along the span of the top facesheet for a two-layered corrugated core {6 × 6} sandwich panel.

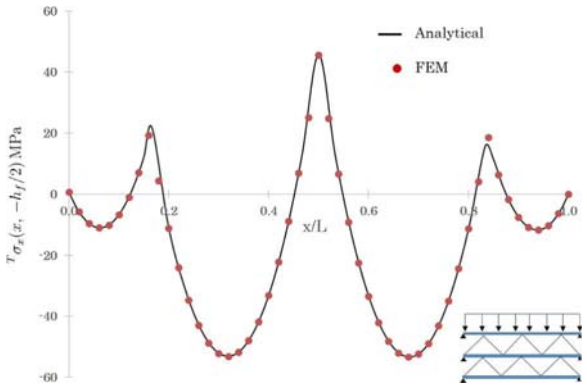

Fig. 6. Variation of the axial stress ${}^{T}\sigma_x(x, -h_f/2)$ along the span of the top facesheet for a two-layered corrugated core {6 × 6} sandwich panel.

Fig. 5 and 6, respectively, show variation of the mid-plane transverse displacement ${}^{T}w_f^0(x)$ and the axial stress ${}^{T}\sigma_x(x, -h_f/2)$ along the span of the top facesheet as obtained from the FE solution and the analytical formulation. The maximum differences of − 0.18 % and − 1.58 %, respectively, in the two values of the transverse displacement and the axial stress occur at $x = L/2$ and $x = 5L/6$, respectively. The deformation and the axial stress results are not symmetric about the mid-span, $x = L/2$, of the panel because of unsymmetric boundary conditions at the two edges. For example, at $x/L = 0.5 \mp 0.025$, the deflection and the axial stress in the top facesheet are 0.157, 0.165 mm and − 45.03, −45.29 MPa, respectively. The analytical model precisely captures the secondary bending of the facesheet between the web plates which manifests as abrupt changes in curvature of the transverse displacement at the facesheet-web plate junctions and as an oscillatory axial stress field with the point of the maximum stress shifting away from the center of the facesheet. A homogenized model of the core does not capture these axial stress fluctuations, and other discrete models [4,6,26] require superposition of a local displacement field on displacements obtained from the homogenized or the global analysis.

In spite of the web plates being very thin, no buckling or other instabilities were observed in the FE solution. The maximum axial compressive load of 5.8 kN is below the critical buckling load of 18.2 kN for a web assumed as a fixed-fixed column. The maximum axial stress of about 60 MPa in a facesheet indicates an axial compressive strain of approximately 10^{-3}.

3.2. Comparison of single-core sandwich panels with corrugated and webcore configurations of equal areal density

3.2.1. Stresses and deflections

The deformations of three single-core sandwich panels with corrugated and webcore configurations, and $L = 0.1$ m, $h_f = 1$ mm, $H = 1$ cm and ${}^{T}q(x) = q_0 = 100$ kN/m are studied. In each case, the thickness t_w of the web plates are adjusted to maintain the core areal density of approximately $0.05\rho_m$ where ρ_m is the mass density of the core material. The areal density ρ_f of the core with n uniformly distributed web plates ($\phi_i = \arctan(nH/L)$ and $\phi_i + \phi_{i+1} = \pi$) is $\rho_f = \frac{nt_w\rho_m}{L\sin(\phi_1)}$, and $\phi_i = 90°$ for the webcore. In Table 1 we have listed core dimensions for 3 corrugated and webcore configurations, arbitrarily chosen, for the study.

Table 1
Dimensions of the corrugated and the webcore configurations for $H = 1$ cm.

Case	n	t_w/h_f	
		Corrugated	Webcore
1	4	0.464	1.25
2	6	0.429	0.833
3	8	0.390	0.625

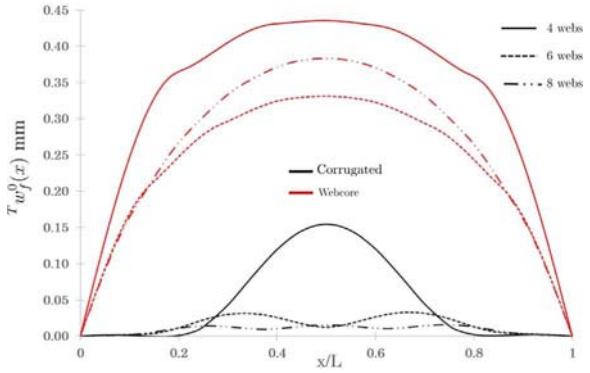

Fig. 7. Variation of the transverse displacement ${}^{T}w_f^0(x)$ along the span of the top facesheet for the corrugated core (in black) and the webcore (in red) single layer sandwich panel. (For interpretation of the references to color in this figure legend, the reader is referred to the web version of this article).

Figs. 7–9 show the variation of the transverse displacement ${}^{T}w_f^0(x)$ and the axial stress ${}^{T}\sigma_x(x, -h_f/2)$ along the span of the top facesheet for the two core configurations. Even though web plates of the corrugated sandwich panel are thinner than those of the webcore configuration, the corrugated sandwich panel has significantly lower top facesheet deflections and axial stresses. For example, for 4 and 6 webs, the central deflection of the top facesheet of the corrugated panel is lesser than that of the webcore panel by 64% and 97%, respectively, while the maximum axial stress in the top facesheet of the corrugated panel is smaller than that of the corresponding webcore panel by 55% and 73%, respectively.

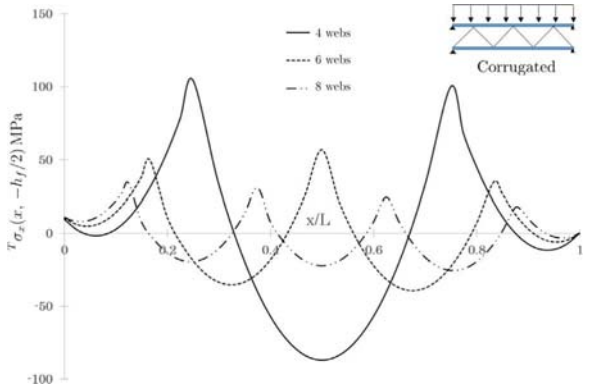

Fig. 8. Variation of the axial stress ${}^{T}\sigma_x(x, -h_f/2)$ along the span of the top facesheet for the single layer corrugated sandwich panel.

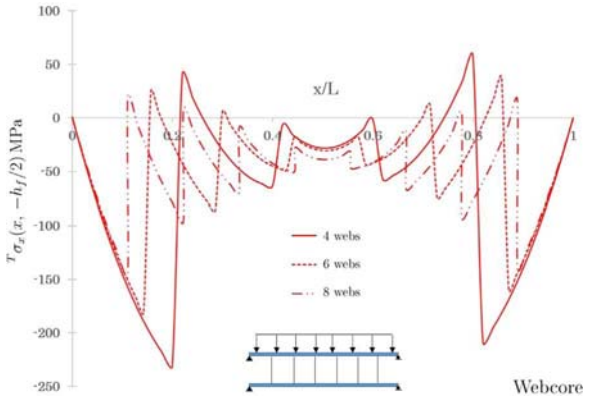

Fig. 9. Variation of the axial stress ${}^{T}\sigma_x(x, -h_f/2)$ along the span of the top facesheet for the single layer webcore sandwich panel.

Furthermore, the waviness in the axial stress field for the webcore panel is more severe than that for the corrugated panel resulting in a discontinuous stress distribution across the webs. It is interesting to note that increasing the number of webs while maintaining a constant areal density in either core configuration decreases the maximum axial stress in the top facesheet but the top facesheet deflections are not monotonically decreasing. For example, for the webcore, increasing the number of webs from 4 to 6 decreases the central deflection of the top facesheet from 0.43 to 0.33 mm but from 6 to 8 causes the central deflection of the top facesheet to increase from 0.33 to 0.38 mm. For the corrugated core, the centroidal deflections of the 6 and 8 webs cases are essentially the same. However, the deflections at other points for 8 webs is smaller than that for the 6 webs case. For 4, 6 and 8 webs in the corrugated core, the maximum axial stress near the left pinned edge is higher than that near the right roller supported edge.

3.2.2. Energies due to axial and bending deformations

We decompose the total elastic strain energy of the i^{th} web into its components due to axial and bending deformations as

$$U^i_{\text{total}} = U^i_{\text{axial}} + U^i_{\text{bending}}$$

where

$$U^i_{\text{axial}} = \frac{1-\nu^2}{2Et_w}\int_0^{H/\sin(\phi_1)} {}^{U}N_i^2(\overline{x})d\overline{x}$$

$$U^i_{\text{bending}} = \frac{12(1-\nu^2)}{2Et_w^3}\int_0^{H/\sin(\phi_1)} {}^{U}M_i^2(\overline{x})d\overline{x}$$

In Tables 2 and 3 we have listed non-dimensionalized values of the strain energy due to axial deformations, $\overline{U}^i_{\text{axial}} = U^i_{\text{axial}}/U^i_{\text{total}}$, the strain energy of bending deformations, $\overline{U}^i_{\text{bending}} = U^i_{\text{bending}}/U^i_{\text{total}}$ as well as the total strain energy, $\overline{U}^i_{\text{total}} = U^i_{\text{total}}/W_n$ in each web plate of the sandwich panels, for the three values of the number of webs. Here, $W_n = \frac{1}{2}\int_0^L {}^{T}q(x)w_f^0(x)dx$ is the work done by the applied load on the sandwich panel. Note that $\overline{U}^i_{\text{axial}}$ and $\overline{U}^i_{\text{bending}}$ equal the fraction of the total strain energy of the i^{th} web that is due to axial and bending deformations, respectively, non-dimensionalized with respect to the total strain energy of the web plate and $W_n = \sum_{i=1}^{n} U^i_{\text{total}} + \sum_{i=1}^{2} U^i_{\text{facesheets}}$. Even though ${}^{T}q(x)$ is kept constant, $w_f^0(x)$ depends upon the core design. Hence, values of W_n depend upon the type of core and the number of webs in the core. Based on these results, the following observations are made:

1. For the core configurations studied, increasing the number of web plates increases the fraction of the work done on the structure that is carried by the core, i.e., the core efficiency. For example, increasing the number of webs from 4 to 8 increases the core efficiency from 20 % to 40 % for the corrugated panel and from 14 % to 66 % for the webcore panel. Furthermore, of the fraction of the work done on the structure that is carried by the core, a significant portion is accounted for by the webs near the supports. For example, for $n = 8$, the webs near the supports carry 58 % and 67 % of the fraction of work done on the structure that is carried by the corrugated core and the webcore, respectively. The large asymmetry in the strain energy distributions in the webs is because the left edge of the facesheets is pinned while the right edge is on a roller. Thus, reaction forces at the two supports are not equal to each other.
2. For corrugated configurations, the web plates mostly deform in compression while for webcore configurations, they deform in bending.
3. For the corrugated (webcore) panel, the work done by the applied surface traction equals 0.25 (1.68), 0.08 (1.21) and 0.05 (1.33) J, respectively, for $n = 4$, 6 and 8, because of the large differences in deflections of the top facesheet that is subjected to the external load;

Table 3
Total strain energy of each web of the webcore sandwich panels. Webs are numbered from the left edge of the panel. $\overline{U}^i_{\text{axial}} = 0$ and $\overline{U}^i_{\text{bending}} = 1$ for each web. $W_4 = 1.68$ J, $W_6 = 1.21$ J and $W_8 = 1.33$ J.

Case 1, $n = 4$		Case 2, $n = 6$		Case 3, $n = 8$	
Web i	$\overline{U}^i_{\text{total}}$	Web i	$\overline{U}^i_{\text{total}}$	Web i	$\overline{U}^i_{\text{total}}$
1	0.07	1	0.20	1	0.23
2	0.00	2	0.04	2	0.09
3	0.00	3	0.01	3	0.03
4	0.06	4	0.00	4	0.00
Total	0.14	5	0.03	5	0.00
		6	0.17	6	0.02
		Total	0.45	7	0.08
				8	0.21
				Total	0.66

Table 2
Axial, bending and total strain energy of each web plate of the corrugated sandwich panels. Web plates are numbered from the left edge of the panel. $W_4 = 0.25$ J, $W_6 = 0.08$ J and $W_8 = 0.05$ J differ because of different deflections of the top facesheet for the three panels.

Case 1, $n = 4$				Case 2, $n = 6$				Case 3, $n = 8$			
Web i	$\overline{U}^i_{\text{axial}}$	$\overline{U}^i_{\text{bending}}$	$\overline{U}^i_{\text{total}}$	Web i	$\overline{U}^i_{\text{axial}}$	$\overline{U}^i_{\text{bending}}$	$\overline{U}^i_{\text{total}}$	Web i	$\overline{U}^i_{\text{axial}}$	$\overline{U}^i_{\text{bending}}$	$\overline{U}^i_{\text{total}}$
1	0.94	0.06	0.12	1	0.99	0.01	0.16	1	0.99	0.01	0.17
2	0.31	0.69	0.01	2	0.95	0.05	0.04	2	0.99	0.01	0.07
3	0.27	0.73	0.01	3	1.00	0.00	0.04	3	1.00	0.00	0.07
4	0.87	0.13	0.05	4	0.99	0.01	0.00	4	1.00	0.00	0.01
Total			0.20	5	0.53	0.47	0.00	5	1.00	0.00	0.01
				6	0.97	0.03	0.06	6	0.99	0.01	0.01
				Total			0.31	7	0.93	0.07	0.01
								8	0.99	0.01	0.06
								Total			0.40

Table 4
Interface forces for each web of the corrugated and the webcore configuration for $n = 6$. Webs are numbered from the left edge of the panel.

Web i	${}^{U}\overline{P}_i^t$ (N)		${}^{D}\overline{Q}_i^t$ (N)		${}^{D}\overline{M}_i^t$ (N-m)	
	Corrugated	Web	Corrugated	Web	Corrugated	Web
1	−10,945	−809	−23	−7742	−0.3	−38.6
2	5501	−694	−24	−3591	−0.3	−18.0
3	−5476	−718	2	−1241	0.1	−6.2
4	−1351	−718	−2	881	−0.1	4.4
5	1359	−694	24	3212	0.3	16.1
6	−6773	−809	20	7231	0.3	36.1

e.g., see Fig. 7.

4. We have listed in Table 4 the interface forces ${}^{U}\overline{P}_i^t$ (along the $\overline{x}-$ direction), ${}^{U}\overline{Q}_i^t$ (along the $\overline{z}-$ direction), and moment ${}^{D}\overline{M}_i^t$ (about the $y-$ axis) acting at the top of each web for the corrugated and the webcore configurations for $n = 6$. The axial compressive force, ${}^{U}\overline{P}_i^t$, in each web plate of the corrugated configuration is significantly larger than that for the webcore configuration. However, the interface moment, ${}^{D}\overline{M}_i^t$, and the force perpendicular to the axis of the web, ${}^{U}\overline{Q}_i^t$, are much larger for the webcore case than that for the corrugated case. Thus, corrugated web plates deform predominantly in axial compression while those of the webcore deform in bending. Furthermore, the significantly lower magnitudes of ${}^{D}\overline{M}_i^t$ for the corrugated case explains the rather smooth variations of the axial stress in the facesheets of the corrugated panel as opposed to the sharp variations of the axial stress observed at the web-facesheet interfaces for the webcore panels. The axial compressive force of 10.9 kN in web 1 of the corrugated panel is considerably less than the Euler buckling load of 143.9 kN when the web is regarded as a fixed-fixed column.

For simply-supported sandwich panels, the data in Tables 2 and 3 indicate that a significant fraction of the work done by the external load on the structure is absorbed as strain energy of deformation of the core plates near the supports. In order to investigate the influence of locations of webs on the sandwich panel deflections, we analyze deformations of a webcore sandwich panel with 2 webs, symmetrically placed at a distance d from the supports, with $L = 0.1$ m, $h_f = 1$ mm, $H = 1$ cm, $t_w = 2.5$ mm and ${}^{T}q(x) = q_0 = 100$ kN/m. Fig. 10 shows the variation of the transverse displacement ${}^{T}w_f^0(x)$ along the span of the top facesheet as d is varied. The top facesheet deflections significantly reduce as the webs are positioned closer to the supports with the maximum deflection reducing by 50% as d is reduced from $L/3$ to $L/8$. These results indicate the potential to optimize the core designs to tailor the response of sandwich panels to fit structural constraints as well as the efficacy of the analytical solution for parametric and design studies.

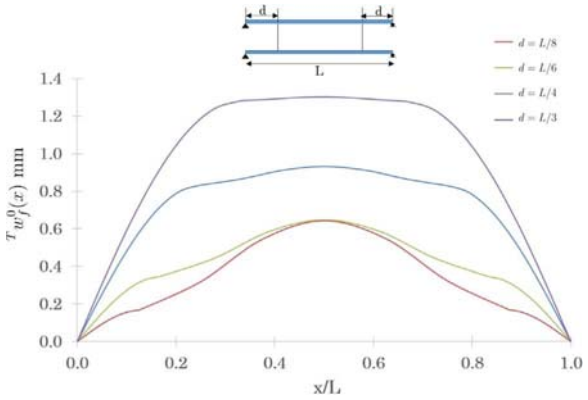

Fig. 10. Influence of locations of webs on the transverse displacement ${}^{T}w_f^0(x)$ along the span of the top facesheet for the webcore single layer sandwich panel. (For interpretation of the references to color in this figure legend, the reader is referred to the web version of this article.)

3.3. Comparison with a homogenization-based approach

We compare results from the present discrete formulation with those from a homogenization-based approach [8] wherein the discrete core is replaced by an equivalent homogeneous orthotropic layer. We study deformations of two single-core corrugated sandwich panels with 6 and 40 webs, respectively, and $L = 0.1$ m, $h_f = 1$ mm, $H = 1$ cm and ${}^{T}q(x) = q_0 = 100$ kN/m. In each case, the thickness t_w of the web plates are adjusted to maintain the core areal density of approximately $0.05\rho_m$. The left ends of the facesheets ($x = 0$) are pinned while the right ends ($x = L$) are supported on rollers. For the homogenization-based approach, the kinematic assumptions of the classical laminate theory are used to analyze the sandwich panel which is modeled as a three-layer laminate with isotropic facesheets of thickness h_f and an orthotropic continuous core of thickness H with equivalent Young's moduli E_x and E_z and Poisson's ratios ν_{xz} and ν_{zx} given as [8]:

$$\begin{aligned} E_x &= \frac{Et_w^3\cos(\phi_i)}{(H^2 - t_w^2\cos^2(\phi_i))H} \\ E_z &= \frac{Et_w^3\sin(\phi_i)}{p^3 - pt_w^2\sin^2(\phi_i)} \\ \nu_{zx} &= \frac{(H^2 + t_w^2\sin^2(\phi_i))\cos^2(\phi_i)}{(H^2 - t_w^2\cos^2(\phi_i))\sin^2(\phi_i)} \\ \nu_{xz} &= \frac{E_z}{E_x}\nu_{zx} \end{aligned} \tag{20}$$

where $p = H\cot(\phi_i)$ and t_w is the thickness of the web plates (see Fig. 2). For the case of a simply supported panel subjected to a uniformly distributed load q_0 on the top surface, the transverse displacement $w(x)$ and the axial stress $\sigma_x(x, z)$ in the panel are determined as

$$\begin{aligned} w(x) &= \frac{q_0 x(x^3 - 2Lx^2 + L^3)}{24D_{33}} \\ \sigma_x(x, z) &= -zQ_{11}\frac{d^2w}{dx^2} \end{aligned} \tag{21}$$

where the equivalent bending stiffness D_{22} of the panel and the constitutive parameter Q_{11} are given by

$$D_{33} = \int_{-(H/2+h_f)}^{-H/2} \frac{E}{1-\nu^2}\,dz + \int_{-H/2}^{H/2} \frac{E_x}{1-\nu_{xz}\nu_{zx}}\,dz + \int_{H/2}^{H/2+h_f} \frac{E}{1-\nu^2}\,dz$$

$$Q_{11} = \begin{cases} \frac{E}{1-\nu^2} & -(H/2 + h_f) \le z \le -H/2 \\ \frac{E_x}{1-\nu_{xz}\nu_{zx}} & -H/2 \le z \le H/2 \\ \frac{E}{1-\nu^2} & H/2 \le z \le H/2 + h_f \end{cases}$$

Figs. 11 and 12 show the variation of the transverse displacement ${}^{T}w_f^0(x) \equiv w(x)$ and the axial stress ${}^{T}\sigma_x(x, -h_f/2) \equiv \sigma_x(x, -(H/2 + h_f))$ along the span of the top facesheet for the two cases as determined by the discrete and the homogenization-based approaches. These results clearly indicate the lack of accuracy of continuum-based models in capturing the displacement and stresses even in panels with a large number (40) of core plates. While the homogenization model is able to qualitatively predict the transverse displacement as the number of webs increase from 6 to 40, it is unable to capture the maximum deflection (error of 25% for the 40 webs case) as well as the abrupt changes in curvature of the facesheets between the webs. As expected, the oscillations in the axial stress field of the facesheets as well as the location of the maximum axial stress cannot be determined by the homogenized model. Furthermore, the displacement and the bending stress are symmetric about the panel center ($x = L/2$). These results demonstrate the importance of using a discrete modeling approach to accurately determine deformations of corrugated core sandwich panels and that the accuracy of the homogenized model depends on the loading and

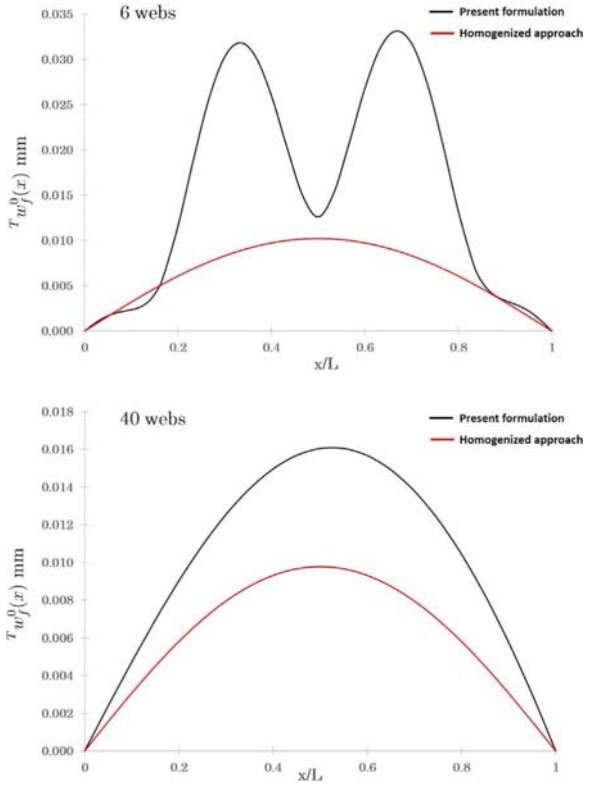

Fig. 11. Variation of the transverse displacement $^T w_f^0(x)$ along the span of the top facesheet for the corrugated core sandwich panel using the present discrete formulation (in black) and a homogenized approach (in red). (For interpretation of the references to color in this figure legend, the reader is referred to the web version of this article).

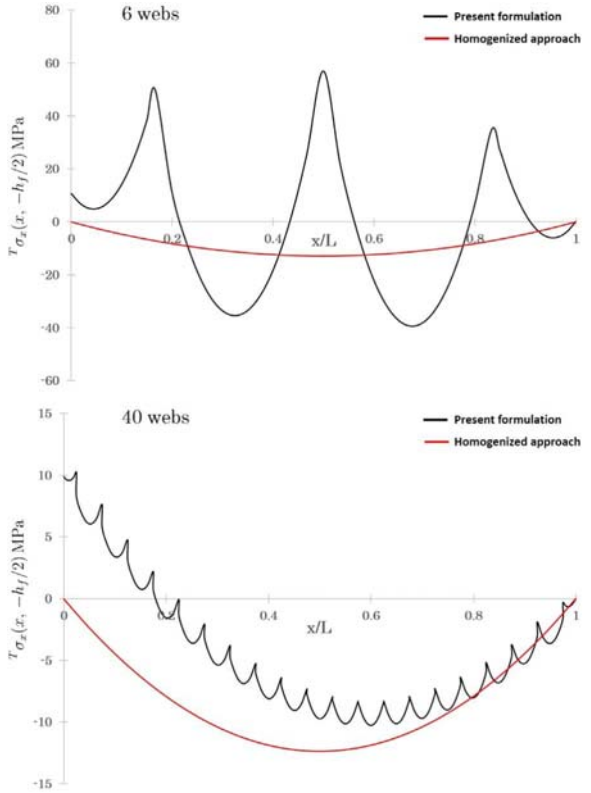

Fig. 12. Variation of the axial stress $^T\sigma_x(x, -h_f/2)$ along the span of the top facesheet for the corrugated core sandwich panel using the present discrete formulation (in black) and a homogenized approach (in red). (For interpretation of the references to color in this figure legend, the reader is referred to the web version of this article).

boundary conditions of the structure.

In order to determine the number of core unit cells required for the possible convergence of results from the homogenization-based solution with those from the discrete approach, we analyzed deformations of a symmetric single-core corrugated sandwich panel with 200 webs of thickness $t_w = 0.25\, h_f$ and dimensions mentioned above. Both ends of the facesheets are assumed to be supported on rollers ($^F w_f^0(0) = {}^F w_f^0(L) = 0$). For the discrete-modeling approach, the symmetry of the deformation field is imposed by the condition $^F u_f^0(L/2) = 0$ for the facesheets. The homogenization-based solution for the displacement and the stress field remains the same and is given by Eqs. (21). Fig. 13 shows the variation of the axial stress $^T\sigma_x(x, -h_f/2) \equiv \sigma_x(x, -(H/2 + h_f))$ along the span of the top facesheet of the sandwich panel as determined by the discrete and the homogenization-based approaches. Clearly, with the increase in core unit cells, the amplitude of waviness of the axial stress in the facesheet decreases and results from the homogenization-based approach are qualitatively similar to those from the discrete model. However, the maximum axial stress at $x = L/2$ is still severely under-predicted by the homogenized model (error of 21%) indicating the need to superimpose a local frame response on the results from the homogenized model, as is done in Refs. [4,26,27], to be able to accurately capture the stresses and deflections in sandwich panels with a large number of core unit cells. It should be noted that we have only considered the homogenization scheme given in Ref. [8] and have not compared the accuracy of other schemes available in the literature. This will be done in a future work.

3.4. Hybrid corrugated-webcore sandwich panels

In Section 3.2 we observed that while the corrugated configuration had lower facesheet deflections, the webcore configuration absorbed a greater fraction of the work done on the structure. In terms of structural

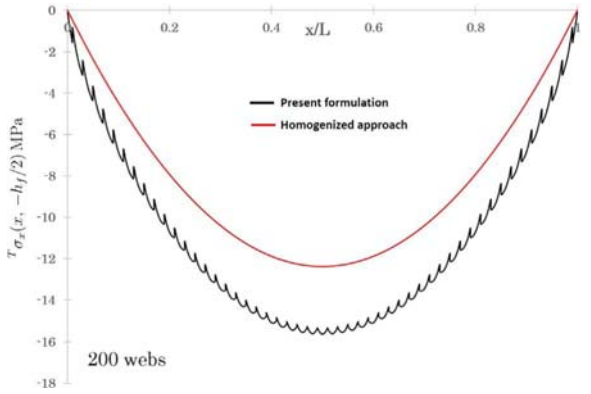

Fig. 13. Variation of the axial stress $^T\sigma_x(x, -h_f/2)$ along the span of the top facesheet for the symmetric corrugated core sandwich panel with 200 webs using the present discrete formulation (in black) and a homogenized approach (in red). (For interpretation of the references to color in this figure legend, the reader is referred to the web version of this article).

efficiency, an ideal sandwich core would be one that absorbs a large fraction of the work done by external forces and lowers values of maximum stresses induced in the structure. In order to delineate advantages, if any, of a hybrid core, we investigate deformations of four hybrid {6 × 6} two-layer sandwich panels designed as a combination of the two core configurations, namely, Corrugated-Corrugated, Corrugated-Web (see Fig. 1), Web-Corrugated and Web-Web wherein the first term denotes the upper core which faces the applied load. In each case, we set $L = 0.1$ m and $h_f = 1$ mm, the core height $H = 1$ cm and the areal density of each core = $0.05\rho_m$. For the corrugated core, the thickness of the web plates $t_w = 0.429\, h_f$, while for the webcore $t_w = 0.833\, h_f$.

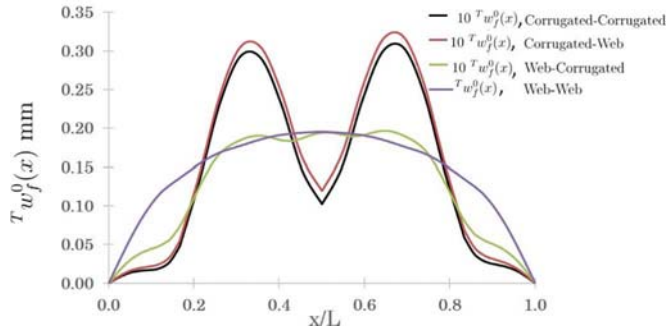

Fig. 14. Variation of the transverse displacement ${}^{T}w_f^0(x)$ along the span of the top facesheet for the hybrid {6 × 6} two-layer sandwich panels. (For interpretation of the references to color in this figure legend, the reader is referred to the web version of this article.)

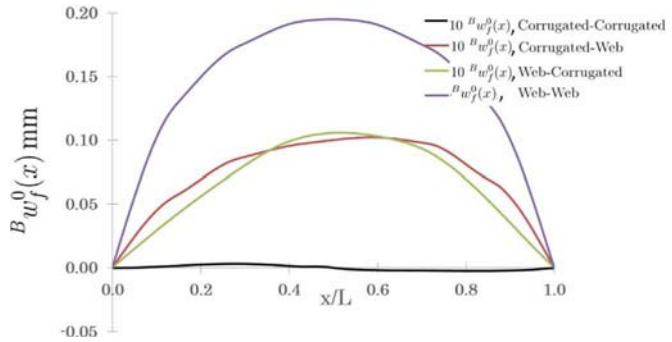

Fig. 15. Variation of the transverse displacement ${}^{B}w_f^0(x)$ along the span of the bottom facesheet for the hybrid {6 × 6} two-layer sandwich panels. (For interpretation of the references to color in this figure legend, the reader is referred to the web version of this article.)

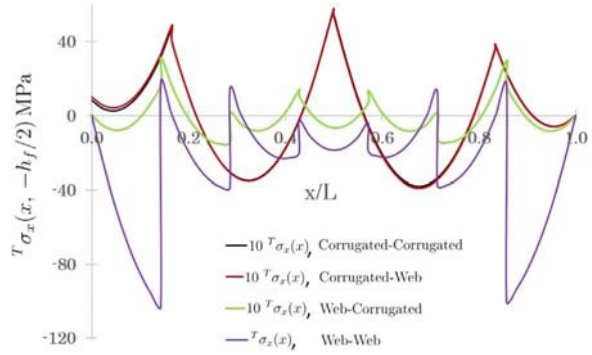

Fig. 16. Variation of the axial stress ${}^{T}\sigma_x(x, -h_f/2)$ along the span of the top facesheet for the hybrid {6 × 6} two-layer sandwich panels. (For interpretation of the references to color in this figure legend, the reader is referred to the web version of this article.)

Figs. 14–17 show the variation of the mid-plane transverse displacement ${}^{D}w_f^0(x)$ and the axial stress ${}^{D}\sigma_x(x, -h_f/2)$ along the span of the top and the bottom facesheets, for the four hybrid sandwich panels. In each case, the deflection and the axial stress values for the Corrugated-Corrugated, Corrugated-Web and Web-Corrugated configurations have been scaled by a factor of 10. In Table 5 we have listed the total strain energy of the core of each hybrid sandwich panel non-dimeniolized with respect to the work done by the applied surface traction for that panel. Based on these results, the following observations are made:

1. The Web-Web combination has the maximum top and bottom facesheet deflections as compared to the other three configurations, as can be seen in Figs. 14 and 15. In sandwich panels with an upper corrugated core, secondary bending effects manifest in the form of steep changes in the curvature between the webs in the top facesheet. However, using a corrugated core in the lower panel does not introduce sudden curvature changes in the bottom facesheet deflections.
2. In the top and the bottom facesheets the maximum axial stress is the largest in the Web-Web combination. Irrespective of the kind of core used in the upper panel, an oscillatory axial stress field is observed in the top facesheet. However, using a corrugated core in the lower panel helps reduce the waviness of the axial stress field in the bottom facesheet. The rather noticeable axial stress in the bottom facesheet near the roller support is due to the horizontal interface force of the web plates meeting the facesheet at the support.
3. As can be seen from the data in Table 5, the fraction of the work done by the external forces absorbed by the cores is greatest for the Web-Corrugated combination. While the energy absorbed by a top corrugated core is larger than that by the corresponding webcore, the efficiency of the second core in such configurations is low. For the Web-Web combination, the work done by the applied surface traction is the maximum with both cores having equal strain energies. This is consistent with the observation that deflections of facesheets in the Web-Web case are the largest amongst the four combinations considered.

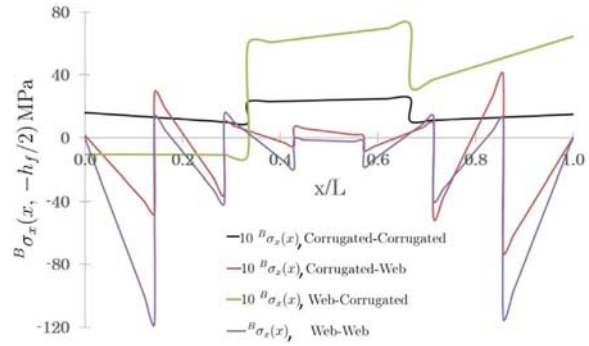

Fig. 17. Variation of the axial stress ${}^{B}\sigma_x(x, -h_f/2)$ along the span of the bottom facesheet for the hybrid {6 × 6} two-layer sandwich panels. (For interpretation of the references to color in this figure legend, the reader is referred to the web version of this article.)

Table 5
Total strain energy of each core (and their sum) of the hybrid two-layer webcore sandwich panels.

Configuration	SE top/Work	SE bot/Work	SE core/Work	Work (J)
Corrugated-Corrugated	0.250	0.008	0.258	0.072
Corrugated-Web	0.292	0.013	0.305	0.077
Web-Corrugated	0.091	0.340	0.431	0.064
Web-Web	0.194	0.197	0.391	0.725

The observations detailed above clearly indicate the need to establish a compromise between conflicting structural constraints. The Web-Corrugated combination would be ideally suited for designs based on core efficiency. However, from a structural integrity standpoint, the Corrugated-Corrugated pattern has significantly lower bottom facesheet deflections and stresses. Each two-layer sandwich plate combination exhibits a qualitatively different mechanical behavior and provides a rich design space to tailor the response to various structural requirements.

4. Remarks

Needless to say, deformations of the facesheets and the cores will depend upon the applied load and the boundary conditions at the panel edges. We have not attempted to find optimal core configurations in this study. For example, one can have a webcore design near the edges

and corrugated core elsewhere or vice versa depending upon the design requirements and applied loads.

5. Conclusions

The cylindrical bending of linearly elastic two-layered corrugated and webcore sandwich panels has been analytically investigated using the mechanics of materials approach. The facesheets and the web plates are analyzed independently using the classical plate theory and the continuity of displacements and tractions at the perfectly bonded web-facesheet interfaces are satisfied. The analytical solution is validated by comparing it with the solution of the linear elasticity equations by the finite element method. Secondary bending effects such as abrupt changes in the curvature of the facesheet between webs and the resulting changes in the axial stress field from being compressive to possibly tensile, that cannot be determined by commonly-used homogenization approaches, are well captured by the model. For a sandwich panel pinned at the left edge and on a roller support at the right edge with a uniformly distributed normal surface traction applied on the top facesheet, the main conclusions are summarized below:

1. By decomposing the total elastic strain energy of the web plates into components due to axial and bending deformations, it is found that the web plates of a corrugated sandwich panel deform in compression while those of a webcore panel deform in bending. Furthermore, a significant fraction of the work done on the structure that is carried by the core is accounted for by webs near the supports.
2. For the four hybrid two-layered sandwich panels studied, the corrugated core designs have the least facesheet deflections and axial stresses while the webcore-based combinations absorb a large fraction of the work done on the structure by the external loads.
3. When the 200 webcore panel is replaced by a homogenized sheet, the maximum axial stress computed using the homogenization-based model is 21% less than that from the discrete model using the mechanics of materials approach and the CPT.

The discrete modeling approach employed here can be extended to multi-layered sandwich panels with an arbitrarily large number of core unit cells. The analytical solutions can be used for parametric and preliminary design studies to tailor the performance of the sandwich panels to varied structural constraints. The prototypes can then be analyzed using computationally expensive numerical simulations for finding details of stresses and strains at critical locations.

Acknowledgments

RCB's work was partially supported by the US Office of Naval Research grant N00014-16-1-2309 to Virginia Polytechnic Institute and State University with Dr. Y.D.S. Rajapakse as the program manager. Views expressed in the paper are those of the authors and neither of ONR nor of Virginia Tech.

References

[1] D. Zenkert, The Handbook of Sandwich Construction, EMAS Publishing, UK, 1997.
[2] T. Fung, K. Tan, T. Lok, Elastic constants for Z-core sandwich panels, J. Struct. Eng. 120 (1994) 3046–3055.
[3] T. Nordstrand, L. Carlsson, H. Allen, Transverse shear stiffness of structural core sandwich, Compos. Struct. 27 (1994) 317–329.
[4] J. Romanoff, P. Varsta, Bending response of web-core sandwich beams, Compos. Struct. 73 (2006) 478–487, http://dx.doi.org/10.1016/j.compstruct.2005.02.018.
[5] J. Romanoff, P. Varsta, Bending response of web-core sandwich plates, Compos. Struct. 81 (2007) 292–302, http://dx.doi.org/10.1016/j.compstruct.2006.08.021.
[6] J. Romanoff, P. Varsta, A. Klanac, Stress analysis of homogenized web-core sandwich beams, Compos. Struct. 79 (2007) 411–422, http://dx.doi.org/10.1016/j.compstruct.2006.02.003.
[7] A. Lebée, K. Sab, Transverse shear stiffness of a chevron folded core used in sandwich construction, Int. J. Solids Struct. 47 (18) (2010) 2620–2629.
[8] H. Wang, S. Chung, Equivalent elastic constants of truss core sandwich plates, J. Press. Vessel Technol. 133 (2011) (041203-1-6).
[9] Y. Xia, M. Friswell, E. Flores, Equivalent models of corrugated panels, Int. J. Solids Struct. 49 (2012) 1453–1462, http://dx.doi.org/10.1016/j.ijsolstr.2012.02.023.
[10] G. Bartolozzi, N. Baldanzini, M. Pierini, Equivalent properties for corrugated cores of sandwich structures: a general analytical method, Compos. Struct. 108 (2014) 736–746, http://dx.doi.org/10.1016/j.compstruct.2013.10.012.
[11] R.K. Boorle, P. Mallick, Global bending response of composite sandwich plates with corrugated core: Part I: effect of geometric parameters, Compos. Struct. 141 (2016) 375–388.
[12] K. Magnucki, E. Magnucka-Blandzi, L. Wittenbeck, Elastic bending and buckling of a steel composite beam with corrugated main core and sandwich faces-Theoretical study, Appl. Math. Model. 40 (2) (2016) 1276–1286.
[13] P. Nilsson, M. Al-Emrani, S.R. Atashipour, Transverse shear stiffness of corrugated core steel sandwich panels with dual weld lines, Thin-Walled Struct. 117 (2017) 98–112.
[14] T. Rabczuk, J. Kim, E. Samaniego, T. Belytschko, Homogenization of sandwich structures, Int. J. Numer. Methods Eng. 61 (7) (2004) 1009–1027.
[15] T.-C. Lin, T.-J. Chen, J.-S. Huang, In-plane elastic constants and strengths of circular cell honeycombs, Compos. Sci. Technol. 72 (12) (2012) 1380–1386.
[16] D. Zangani, M. Robinson, A. Gibson, Evaluation of stiffness terms for Z-cored sandwich panels, Appl. Compos. Mater. 14 (3) (2007) 159–175.
[17] N. Buannic, P. Cartraud, T. Quesnel, Homogenization of corrugated core sandwich panels, Compos. Struct. 59 (3) (2003) 299–312.
[18] W. Burton, A. Noor, Assessment of computational models for sandwich panels and shells, Comput. Methods Appl. Mech. Eng. 124 (1995) 125–151.
[19] W. Burton, A. Noor, Assessment of continuum models for sandwich panel honeycomb cores, Comput. Methods Appl. Mech. Eng. 145 (1997) 341–360.
[20] A. Pydah, K. Bhaskar, An accurate discrete model for web-core sandwich plates, J. Sandw. Struct. Mater. 18 (4) (2016) 474–500.
[21] Q.H. Cheng, H. Lee, C. Lu, A numerical analysis approach for evaluating elastic constants of sandwich structures with various cores, Compos. Struct. 74 (2006) 226–236, http://dx.doi.org/10.1016/j.compstruct.2005.04.007.
[22] S. Heimbs, Virtual testing of sandwich core structures with LS-Dyna, in: Proceedings of the 26th CADFEM Users Meeting, Darmstadt, 2008.
[23] S. Heimbs, Virtual testing of sandwich core structures using dynamic finite element simulations, Comput. Mater. Sci. 45 (2) (2009) 205–216.
[24] S. Heimbs, Foldcore sandwich structures and their impact behaviour: an overview, in: Dynamic Failure of Composite and Sandwich Structures, Springer, 2013, pp. 491–544.
[25] S. Fischer, Realistic FE simulation of foldcore sandwich structures, Int. J. Mech. Mater. Eng. 10 (1) (2015) 1–11.
[26] J. Liu, Y. Cheng, R. Li, F. Au, A semi-analytical method for bending, buckling, and free vibration analyses of sandwich panels with square-honeycomb cores, Int. J. Struct. Stab. Dyn. 10 (2010) 127–151, http://dx.doi.org/10.1142/S0219455410003361.
[27] L. He, Y. Cheng, J. Liu, Precise bending stress analysis of corrugated-core, honeycomb-core and X-core sandwich panels, Compos. Struct. 94 (2012) 1656–1668, http://dx.doi.org/10.1016/j.compstruct.2011.12.033.
[28] A. Pydah, K. Bhaskar, Accurate analytical solutions for shear-deformable web-core sandwich plates, J. Sandw. Struct. Mater. 0(0), ⟨http://dx.doi.org/10.1177/1099636216632452⟩.
[29] C. Weeks, C. Sun, Multi-core composite laminates, J. Adv. Mater. 25 (3) (1994) 28–37.
[30] S. Heimbs, P. Middendorf, S. Kilchert, A.F. Johnson, M. Maier, Experimental and numerical analysis of composite folded sandwich core structures under compression, Appl. Compos. Mater. 14 (5–6) (2007) 363–377.
[31] Z. Wang, Q. Xu, Experimental research on soundproof characteristics for the sandwich plates with folded core, J. Vib. Eng. 19 (1) (2006) 65–69.
[32] V. ABAQUS, 6.14 Documentation, Dassault Systemes Simulia Corporation.